PROCEEDINGS OF SPIE

SPIEDigitalLibrary.org/conference-proceedings-of-spie

Detecting aggressive papillary thyroid carcinoma using hyperspectral imaging and radiomic features

Leitch, Ka'Toria, Halicek, Martin, Shahedi, Maysam, Little, James, Chen, Amy, et al.

Ka'Toria Leitch, Martin Halicek, Maysam Shahedi, James V. Little, Amy Y. Chen, Baowei Fei, "Detecting aggressive papillary thyroid carcinoma using hyperspectral imaging and radiomic features," Proc. SPIE 12033, Medical Imaging 2022: Computer-Aided Diagnosis, 1203322 (4 April 2022); doi: 10.1117/12.2611842

SPIE.

Event: SPIE Medical Imaging, 2022, San Diego, California, United States

Detecting Aggressive Papillary Thyroid Carcinoma Using Hyperspectral Imaging and Radiomic Features

Ka'Toria Leitch[1], Martin Halicek[1], Maysam Shahedi[1], James V. Little[2], Amy Y. Chen[3], Baowei Fei [1,4,*]

[1] Department of Bioengineering, University of Texas at Dallas, Richardson, TX
[2] Department of Pathology and Laboratory Medicine, Emory University School of Medicine, Atlanta, GA
[3] Department of Otolaryngology, Emory University School of Medicine, Atlanta, GA
[4] Department of Radiology, The University of Texas Southwestern Medical Center, Dallas, TX
*E-mail: bfei@utdallas.edu, website: https://fei-lab.org

ABSTRACT

Hyperspectral imaging (HSI) and radiomics have the potential to improve the accuracy of tumor malignancy prediction and assessment. In this work, we extracted radiomic features of fresh surgical papillary thyroid carcinoma (PTC) specimen that were imaged with HSI. A total of 107 unique radiomic features were extracted. This study includes 72 *ex-vivo* tissue specimens from 44 patients with pathology-confirmed PTC. With the dilated hyperspectral images, the shape feature of least axis length was able to predict the tumor aggressiveness with a high accuracy. The HSI-based radiomic method may provide a useful tool to aid oncologists in determining tumors with intermediate to high risk and in clinical decision making.

Keywords: Head, Neck Cancer, Radiomics, Hyperspectral Imaging, Tissues, Tumor Aggression

1. INTRODUCTION

Papillary thyroid carcinoma (PTC) is the most common form of differentiated thyroid cancers [1]. PTC accounts for approximately 80% of thyroid cancer cases [2,3]. PTC is not only the most common form of thyroid cancer but also among the most malignant. PTC is particularly known for its high lymph node metastasis rate, where 20-50% of patients will experience central lymph node metastasis [1]. Of individuals diagnosed with PTC, approximately one in four will not surpass the five-year survival mark [4]. The primary reason metastasis occurs is due to the invasion of the lymphatic system by the disease [5]. Individuals who undergo tumor resection as a therapy for PTC have recurrent disease nearly a third of the time [6]. 35% of individuals who suffer from recurrent disease, approximately 1 and 10 of those diagnosed, die from the cancer [7]. Tumor aggressiveness is routinely determined during pathological evaluation of papillary thyroid tissue specimens via fine-needle biopsy in conjunction with preoperative notes [8]. Many fine-needle biopsies have inconclusive results, which leads to inefficient treatment of aggressive PTC tumors. Inefficient treatment is partly due to the incomplete resection of tumors [1].

In our early work, radiomics has been used to predict PTC aggression with an AUC of 0.85 [9]. Machine learning techniques, such as convolutional neural networks, were demonstrated to be effective at detecting head and neck cancer using hyperspectral imaging (HSI) [10-15]. A previous study classified the presence of PTC metastasis on ultrasound with an AUC of 0.73 based on clinical features such as age and tumor stage that were outlined in the pathological report [16]. One research group utilized radiomics on multiparametric MRI to determine extrathyroidal extension, a common feature of aggressive PTC. This group was able to predict extrathyroidal extension on PTC tumors with an AUC of 0.87 [17]. To the best of our knowledge, this is the first work to investigate tumor aggressiveness classification of PTC utilizing radiomics on hyperspectral images.

2. METHODS

2.1 Hyperspectral Imaging

The HSI data were acquired from 72 *ex-vivo* fresh surgical tissue specimens of 44 patients undergoing routine resection of papillary thyroid tumors. The data acquisition and system were described in our previous studies [8-9,18-22]. The

Medical Imaging 2022: Computer-Aided Diagnosis, edited by Karen Drukker, Khan M. Iftekharuddin, Hongbing Lu, Maciej A. Mazurowski, Chisako Muramatsu, Ravi K. Samala, Proc. of SPIE
Vol. 12033, 1203322 · © 2022 SPIE · 1605-7422 · doi: 10.1117/12.2611842

spectral range is from 450 nm to 900 nm. The image size is 1040×1392×91 pixels (height × width × spectral bands) where there is a 25 μm per pixel spatial resolution. The scanning duration for each specimen was approximately one minute.

2.2 Papillary Thyroid Carcinoma Tissue Database

The tissue specimens included two different tissue types: tumor only and tumor/normal interface tissue. We acquired the tissue from the primary tumor as well as tissue located at the tumor/normal margin. The tumor/normal margin, which contained both tumor and normal tissue, was included to determine the effects of tumor boundaries on the effectiveness of this classification tool. Tumor and normal tissue were outlined by a board-certified pathologist. After excluding benign tumors, 39 tumor and 33 tumor/normal specimens were selected for this investigation. Pathological reports outlining patient characteristics were also provided after the redaction of personally identifiable information.

PTC tumor aggressiveness was defined according to the American Thyroid Association (ATA) 2015 Risk Stratification System for differentiating thyroid carcinomas [9, 15, 22]. We classified aggressive tumors to include tumors that would be identified as intermediate-risk or high-risk by the ATA. PTC tumors are categorized as intermediate-risk or high-risk by exhibiting one or more of the following histopathological features: aggressive histologic subtype (*e.g.,* tall cell, hobnail, columnar cell), vascular invasion, tumor capsular invasion, extra-thyroidal extension (ETE), regional metastases, or distant metastases. Alternatively, non-aggressive, *i.e.,* low-risk, PTC tumors were classified as tissues that did not containing aggressive features. The histopathological features were annotated in the corresponding pathological reports. Of the 44 patients, 35 were classified as aggressive, and nine were classified as non-aggressive. This corresponds to 58 aggressive and 14 non-aggressive tissue specimens. For this study, we grouped tissues into four distinct groups. These four groups are (1) aggressive tumor/normal interface tissue, (2) non-aggressive tumor/normal interface tissue, (3) aggressive tumor tissue, and (4) non-aggressive tumor tissue.

2.3 Preprocessing of Hyperspectral Images

HSI of the tumors were dilated using 5, 10, 15, and 20 pixels where the spatial resolution is 25 μm per pixel. This procedure was performed in MATLAB (MathWorks, Inc., Natrick, MA). Dilation has the effect of emphasizing the portion of the tumor that overlaps with the normal tissue, as shown in gray below in Figure 1. Since extrathyroidal extension is an indicator of tumor metastasis and aggression, emphasizing the tumor/normal interface region intensifies the effect of radiomic features in that area. As a result, detection of image features indicative of tumor aggression may be suspected.

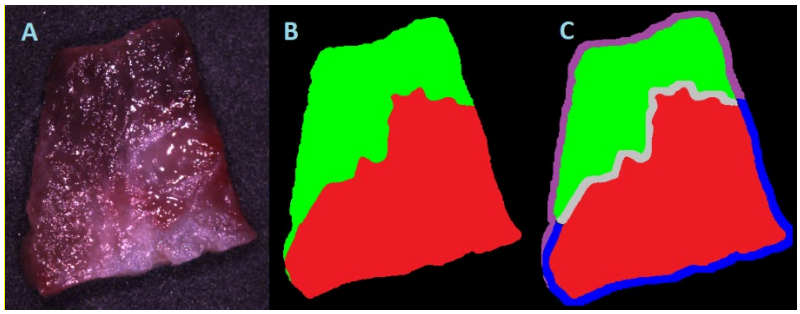

Figure 1. Example of tumor/normal interface tissue represented as an HSI-synthesized RGB image (A), the mask of the tumor is shown in red (B) and the normal tissue is shown in green (B), and the result of 20-pixel dilation on the tumor mask is shown in blue (C), the normal mask is shown in purple (C), and the overlap of the tumor and normal masks is shown in gray (C).

2.3 Radiomic Feature Extraction and Selection

Both non-dilated and dilated HSI were loaded into the PyRadiomics package where 107 unique features were extracted [23]. PyRadiomics calculates shape, first-order, and texture features. Texture features include gray-level dependence matrix, gray-level co-occurrence matrix, gray-level run length matrix, and gray-level size zone matrix, and

neighboring gray tone dependence matrix features. These included 18 first order, 14 shape-based, 14 gray-level dependence matrix, 24 gray-level co-occurrence matrix, 16 gray-level run length matrix, 16 gray-level size zone matrix, and 5 neighboring gray tone dependence matrix features. These feature definitions were established by the Imaging Biomarker Standardization Initiative (IBSI) [24].

After feature extraction, radiomic feature selection was performed. The purpose of feature selection is to avoid issues presented by high dimensionality, algorithm performance, noisy or ambiguous data, and replicability of the study [25]. The goal of feature selection is to identify the relationship between the radiomic feature(s) and the presence of tumor aggression by defining the feature(s) that largely impact, or create dependency, on the outcome of aggressive or non-aggressive [26]. Five feature selection methods were implemented: analysis of variance (ANOVA), forward elimination, backward elimination, and Pearson correlation. These feature selection methods can be categorized into three types of feature selection tools: filter, wrapper, and embedded. Filter methods are useful due to their quick computation time and intolerance to overfitting. The wrapper feature selection tools are forward and backward elimination. In wrapper methods, features are chosen by analyzing subsets of variables that allows detection of interaction among variables in addition to their relationship to the prediction variable. Lastly, LASSO is an example of an embedded feature selection tool. This method works by combining filter and wrapper methods into a learning algorithm [27-30].

2.4 Feature Extraction and Classification

Eighteen classification algorithms were tested for each of the five feature extraction methods and five dilation groups (0, 5, 10, 15, 20 pixels) for a total of 450 combinations. All classification algorithms were implemented using the python scikit-learn package [25]. Classifiers were trained using an independent training set (N = 54 specimens). The predictive performance was evaluated based on an independent testing set (N = 18 specimens) using accuracy analysis. Both the independent training and testing sets were randomly selected on a patient basis. We did not implement a validation set because our training set achieved 100% accuracy. Each dilation group was tested within the group. For example, a 5-pixel dilated training set was used to train the algorithm for the 5-pixel dilated testing set. No patient overlaps occurred between the training and testing groups.

3. RESULTS

PTC aggression was classified with an accuracy of 100% for patients when any of the four dilation groups ((5, 10, 15, 20 pixels). Without dilation, the accuracy was 83.3%, indicating the importance of the preprocessing step. The most important feature selected by each feature selection algorithm according to the different levels of dilation is outlined in Table 1. The number of features chosen by the respective feature selection algorithms is in parentheses in Column 1 of Table 1. Table 1 illustrates that least axis length was chosen as the most important feature frequently. Figure 2 shows that the feature selection methods lead to similar results regardless of the classification method.

Table 1. The most important radiomic feature in relationship to the different feature selection methods and corresponding image dilation size. Least axis length is the most prevalent feature.

	DILATION (pixels)			
METHODS	5	10	15	20
ANOVA (11)	Surface Volume Ratio	Least Axis Length	Least Axis Length	Least Axis Length
LASSO (12-15)	Surface Area	Surface Volume Ratio	Maximum 2D Diameter Row	Long Run Low Gray Level Emphasis
Forward Elimination (103)	Surface Volume Ratio	Least Axis Length	Least Axis Length	Least Axis Length
Backward Elimination (99)	Surface Volume Ratio	Least Axis Length	Least Axis Length	Least Axis Length
Pearson Correlation (26)	Surface Volume Ratio	Least Axis Length	Least Axis Length	Least Axis Length

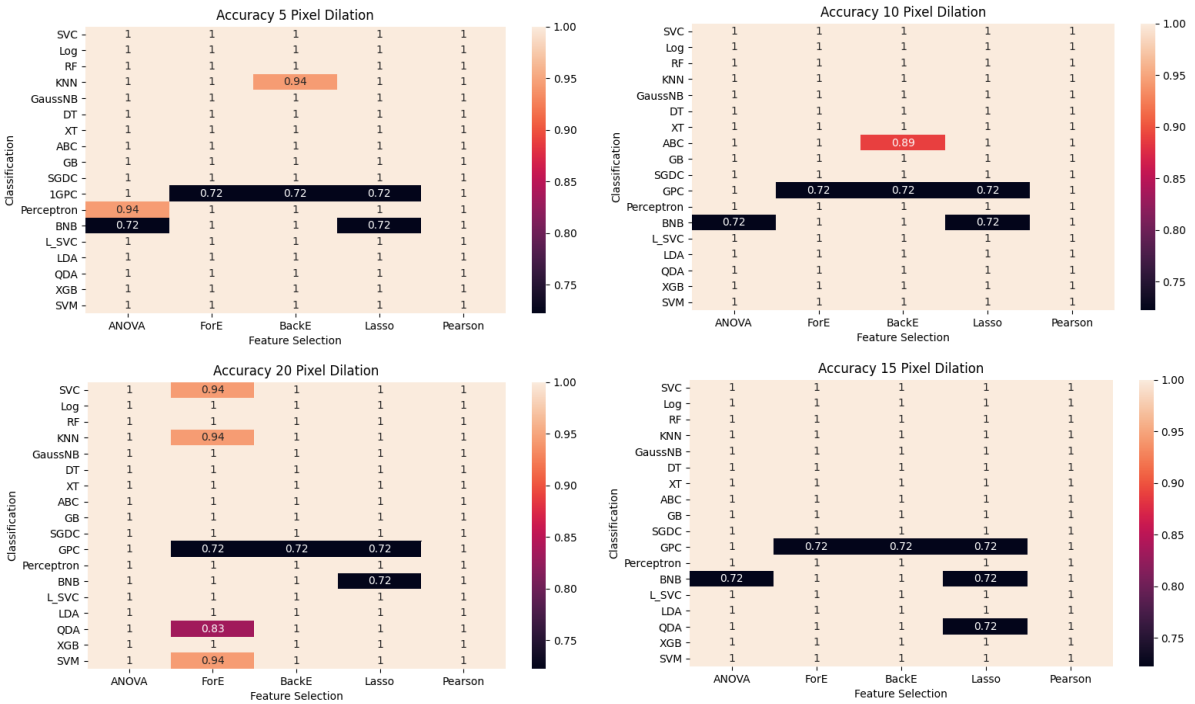

Figure 2. Heatmaps displaying embedded accuracy values for four dilation testing groups: 5 pixel (top-left), 10 pixel (top-right), 20 pixel (bottom-left), 1and 5 pixel (bottom-right). The feature selection methods (column) and classification tools (row) with a maximum accuracy of 1.00 are shown. Acronyms are outlined in Table 2.

Table 2. Abbreviation for the methods

Acronym	Method
SVC	Support-Vector Classifier
Log	Logarithmic
RF	Random Forest
KNN	K- Nearest Neighbor
GaussNB	Gaussian Naïve Bayes
DT	Decision Trees
XT	Extra Trees
ABC	AdaBoost Classifier
GB	Gradient Boosting
SGDC	Stochastic Gradient Descent
GPC	Gaussian Process Classification
BNB	Bernoulli Naïve Bayes
L_SVC	Linear Support-Vector Classifier
LDA	Linear Discriminant Analysis
QDA	Quadratic Discriminant Analysis
XBG	eXtreme Gradient Boosting
SVM	Support-Vector Machine
ANOVA	Analysis of Variance
LASSO	Least Absolute Shrinkage and Selection Operator
Ridge Reg	Ridge Regression

Of the features selected, least axis length was chosen as an important feature most often when classifying PTC tumor aggression. This feature is the smallest axis length of the region of interest enclosing ellipsoid and is calculated using the largest principal component [23]. A paired student's t-test showed that the least axis length is significantly different between aggressive and non-aggressive specimens ($p < 0.05$) after the dilation processing.

Figure 3 shows the distribution of the principal components for all non-dilated HSI. Aggressive tumor tissue has a higher frequency surrounding a coefficient value of 0.3 than non-aggressive tumor tissue (Figure 4). Aggressive tumor at the tumor/normal interface is centered around a coefficient value of approximately 0.35, and non-aggressive tumor/normal tissue is centered around a coefficient value of approximately 0.25 (Figure 5).

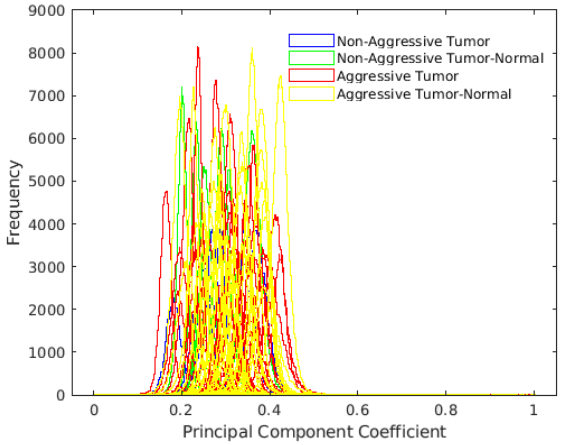

Figure 3. Histograms of the principal component coefficients of all specimens.

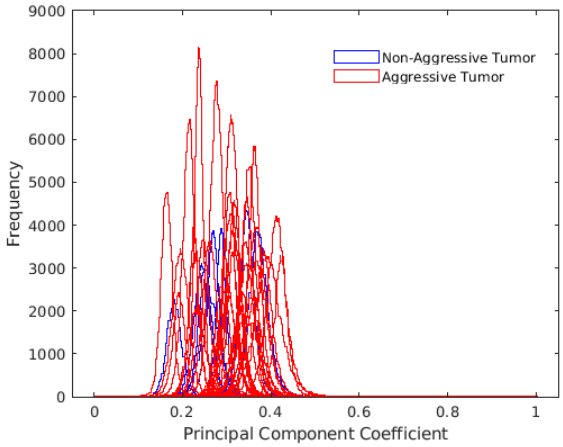

Figure 4. Histograms of the principal component coefficients of tumor specimens. Aggressive tumor specimens have a higher principal component coefficient frequency than non-aggressive tumor specimen around 0.3.

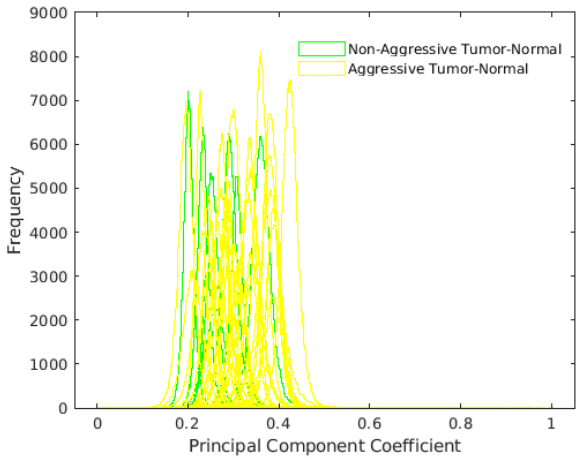

Figure 5. Histograms of the principal component coefficients of tumor/normal interface specimens. Aggressive tumor/normal interface specimens are centered around a higher principal component coefficient of approximately 0.35, and non-aggressive tumor/normal interface specimens are centered around a lower principal component coefficient of approximately 0.25.

4. DISCUSSION & CONCLUSION

In this work, we present a hyperspectral radiomic method for tumor aggressiveness classification. To the best of our knowledge, this is the first work to investigate tumor aggressiveness classification of PTC utilizing hyperspectral images. In this preliminary study, PTC tumor aggression was independently classified with an accuracy of 100% when image dilation was applied to HSI. Least axis length, a principal component shape-based feature, is a highly significant radiomic feature when determining PTC aggression on dilated HSI.

An important limitation of this study is the small data set. The number of patients (N=44) may not be sufficient to generalize the applicability of this study in a clinical environment. Although we implemented an independent testing set, we cannot conclude that this data is representative of all cases that may be presented. In addition, the number of aggressive tissue specimen (N = 58) was much larger than the number of non-aggressive tissue specimen (N = 14).

Least axis length is correlated to the largest principal component of an image, which can be considered as the attribute that is most essential to describing that image. It may correspond to morphological features within the respective tissue specimen. For HSI data, least axis length may be linked to the spectral information of the PTC tissues. More studies are required in order to explain this radiomic feature and its association with aggressive PTC. Nevertheless, this work demonstrates the potential of HSI radiomics for the classification of PTC tumor aggressiveness, which may provide an automatic tool to aid oncologists in clinical decision making.

ACKNOWLEDGEMENTS

This research was supported in part by the U.S. National Institutes of Health (NIH) grants (R01CA156775, R01CA204254, R01HL140325, and R21CA231911) and by the Cancer Prevention and Research Institute of Texas (CPRIT) grant RP190588.

REFERENCES

[1] Rui, Z.Y., Liu, Y., Zheng, W. et al. A retrospective study of the risk factors and the prognosis in patients with papillary thyroid carcinoma depending on the number of lymph node metastasis. Clin Exp Med 21, 277–286. https://doi.org/10.1007/s10238-020-00675-8 (2021).

[2] Bikas A., Burman K.D. Epidemiology of Thyroid Cancer. In: Luster M., Duntas L., Wartofsky L. (eds) The Thyroid and Its Diseases. Springer, Cham (2019).

[3] Guo, Zhenying MD*,†; Ge, Minghua MD*,†; Chu, Ying-Hsia MD‡; Asioli, Sofia MD§; Lloyd, Ricardo V. MD, PhD‡ Recent Advances in the Classification of Low-grade Papillary-like Thyroid Neoplasms and Aggressive Papillary Thyroid Carcinomas: Evolution of Diagnostic Criteria, Advances In Anatomic Pathology: July - Volume 25 - Issue 4 - p 263-272 doi: 10.1097/PAP.0000000000000198 (2018).

[4] American Cancer Society. Cancer Facts & Figures 2021. Atlanta: American Cancer Society; (2021).

[5] Limaiem F, Rehman A, Mazzoni T. Papillary Thyroid Carcinoma. [Updated 2021 Jul 11]. In: StatPearls [Internet]. Treasure Island (FL): StatPearls Publishing; 2021 Jan-. Available from: https://www.ncbi.nlm.nih.gov/books/NBK536943/(2021).

[6] Ywata de Carvalho A, Kohler HF, Gomes CC, Vartanian JG, Kowalski LP. Predictive factors for recurrence of papillary thyroid carcinoma: analysis of 4,085 patients. Acta Otorhinolaryngol Ital. 2021;41(3):236-242. doi:10.14639/0392-100X-N1412 (2021).

[7] Song, Eyun, Min Ji Jeon, Hye-Seon Oh, Minkyu Han, Yu-Mi Lee, Tae Yong Kim, Ki-Wook Chung, Won Bae Kim, Young Kee Shong, Dong Eun Song, and Won Gu Kim. "Do aggressive variants of papillary thyroid carcinoma have worse clinical outcome than classic papillary thyroid carcinoma?". *European Journal of Endocrinology* 179.3: 135-142. < https://doi.org/10.1530/EJE-17-0991>. Web. 29 Jun. (2020).

[8] Martin Halicek, James D. Dormer, James V. Little, Amy Y. Chen, and Baowei Fei, "Tumor detection of the thyroid and salivary glands using hyperspectral imaging and deep learning," Biomed. Opt. Express 11, 1383-1400 (2020)

[9] Ka'Toria Edwards, Martin Halicek, James V. Little, Amy Y. Chen, Baowei Fei, "Multiparametric radiomics for predicting the aggressiveness of papillary thyroid carcinoma using hyperspectral images," Proc. SPIE 11597, Medical Imaging 2021: Computer-Aided Diagnosis, 1159728 (15 February 2021); https://doi.org/10.1117/12.2582147 (2021).

[10] Ortega S, Halicek M, Fabelo H, Camacho R, Plaza MD, Godtliebsen F, M Callicó G, Fei BW (Corresponding author). Hyperspectral imaging for the detection of glioblastoma tumor cells in H&E slides using convolutional neural networks. Sensors; 20(7):1911.(2020).

[11] Ma L, Halicek M, Fei BW. In vivo cancer detection in animal model using hyperspectral image classification with wavelet feature extraction. Medical Imaging 2020: Biomedical Applications in Molecular, Structural, and Functional Imaging; 11317(113171C). International Society for Optics and Photonics (2020).

[12] Ortega S, Halicek M, Fabelo H, Guerra R, Lopez C, Lejeune M, Godtliebsen F, Callico GM, Fei BW (Corresponding author). Hyperspectral imaging and deep learning for the detection of breast cancer cells in digitized histological images. Medical Imaging 2020: Digital Pathology; 11320(113200V). International Society for Optics and Photonics, (2020).

[13] Ma L, Halicek M, Zhou X, Dormer J, Fei BW (Corresponding author). Hyperspectral microscopic imaging for automatic detection of head and neck squamous cell carcinoma using histologic image and machine learning. Medical Imaging 2020: Digital Pathology; 11320(113200W). International Society for Optics and Photonics, (2020).

[14] Halicek M, Little JV, Wang X, Chen AY, Fei B. Optical biopsy of head and neck cancer using hyperspectral imaging and convolutional neural networks. J Biomed Opt. 2019 Mar;24(3):1-9. doi: 10.1117/1.JBO.24.3.036007. PMID: 30891966; PMCID: PMC6975184 (2019).

[15] Halicek M, Lu G, Little JV, Wang X, Patel M, Griffith CC, El-Deiry MW, Chen AY, Fei B. Deep convolutional neural networks for classifying head and neck cancer using hyperspectral imaging. J Biomed Opt. 2017 Jun 1;22(6):60503. doi: 10.1117/1.JBO.22.6.060503. PMID: 28655055; PMCID: PMC5482930 (2017).

[16] Zou Y, Shi Y, Liu J, et al. A Comparative Analysis of Six Machine Learning Models Based on Ultrasound to Distinguish the Possibility of Central Cervical Lymph Node Metastasis in Patients With Papillary Thyroid Carcinoma. Front Oncol. 2021;11:656127. Published 2021 Jun 25. doi:10.3389/fonc.2021.656127 (2021).

[17] Wei, R., Wang, H., Wang, L. et al. Radiomics based on multiparametric MRI for extrathyroidal extension feature prediction in papillary thyroid cancer. BMC Med Imaging 21, 20 (2021). https://doi.org/10.1186/s12880-021-00553-z (2021).

[18] Zhang, Y., Wu, X., He, L., Meng, C., Du, S., Bao, J., & Zheng, Y. (2020). Applications of hyperspectral imaging in the detection and diagnosis of solid tumors. Translational Cancer Research, 9(2), 1265-1277. doi:10.21037/tcr.2019.12.53 (2020)

[19] Halicek M, Fabelo H, Ortega S, Callico GM, Fei B. In-Vivo and Ex-Vivo Tissue Analysis through Hyperspectral Imaging Techniques: Revealing the Invisible Features of Cancer. *Cancers (Basel)*.;11(6):756. Published 2019 May 30. doi:10.3390/cancers11060756 (2019).

[20] Fei B, Lu G, Wang X, Zhang H, Little JV, Patel MR, Griffith CC, El-Diery MW, Chen AY. Label-free reflectance hyperspectral imaging for tumor margin assessment: a pilot study on surgical specimens of cancer patients. J Biomed Opt. 2017 Aug;22(8):1-7. doi: 10.1117/1.JBO.22.8.086009. PMID: 28849631; PMCID: PMC5572439 (2017).

[21] Lu G, Little JV, Wang X, Zhang H, Patel MR, Griffith CC, El-Deiry MW, Chen AY, Fei B. Detection of Head and Neck Cancer in Surgical Specimens Using Quantitative Hyperspectral Imaging. Clin Cancer Res. 2017 Sep 15;23(18):5426-5436. doi: 10.1158/10780432.CCR-17-0906. Epub 2017 Jun 13. PMID: 28611203; PMCID: PMC5649622 (2017).

[22] Halicek M, Fabelo H, Ortega S, Little JV, Wang X, Chen AY, Callico GM, Myers L, Sumer BD, Fei B. Hyperspectral imaging for head and neck cancer detection: specular glare and variance of the tumor margin in surgical specimens. J Med Imaging (Bellingham). 2019 Jul;6(3):035004. doi: 10.1117/1.JMI.6.3.035004. Epub 2019 Sep 14. PMID: 31528662; PMCID: PMC6744927 (2019).

[23] Griethuysen, J. J. M., Fedorov, A., Parmar, C., Hosny, A., Aucoin, N., Narayan, V., Beets-Tan, R. G. H., Fillon-Robin, J. C., Pieper, S., Aerts, H. J. W. L. (2017). Computational Radiomics System to Decode the Radiographic Phenotype. Cancer Research, 77(21), e104– e107. `https://doi.org/10.1158/0008-5472.CAN-17-0339 https://doi.org/10.1158/0008-5472.CAN-17-0339 (2017).

[24] Zwanenburg, A., Leger, S., Vallières, M., and Löck, S. (2016). Image biomarker standardisation initiative - feature definitions. In eprint arXiv:1612.07003 [cs.CV] (2016).

[25] Scikit-learn: Machine Learning in Python, Pedregosa et al., JMLR 12, pp. 2825-2830, (2011).

[26] Dhal, P., Azad, C. A comprehensive survey on feature selection in the various fields of machine learning. Appl Intell (2021). https://doi.org/10.1007/s10489-021-02550-9 (2021).

[27] Hamon, Julie (November 2013). Optimisation combinatoire pour la sélection de variables en régression en grande dimension : Application en génétique animale (Thesis) (in French). Lille University of Science and Technology. (2013)

[28] Yu, Lei; Liu, Huan (August 2003). "Feature selection for high-dimensional data: a fast correlation-based filter solution"(PDF). ICML'03: Proceedings of the Twentieth International Conference on International Conference on Machine Learning: 856–863. (2003)

[29] T. M. Phuong, Z. Lin et R. B. Altman. Choosing SNPs using feature selection. Archived 2016-09-13 at the Wayback Machine Proceedings / IEEE Computational Systems Bioinformatics Conference, CSB. IEEE Computational Systems Bioinformatics Conference, pages 301-309, 2005. PMID 16447987. (2005)

[30] Saghapour E, Kermani S, Sehhati M. A novel feature ranking method for prediction of cancer stages using proteomics data. PLoS One. 2017 Sep 21;12(9):e0184203. doi: 10.1371/journal.pone.0184203. PMID: 28934234; PMCID: PMC5608217. (2017)